AGU PUBLICATIONS

Geophysical Research Letters

RESEARCH LETTER
10.1002/2013GL058818

Key Points:
- Geoengineering aerosol would prolong the westerly phase of the QBO
- Large geoengineering stratospheric aerosol injections might interrupt the QBO
- QBO changes are due to aerosol warming and increased residual vertical velocity

Supporting Information:
- Readme
- Figures S1–S7

Correspondence to:
V. Aquila,
valentina.aquila@jhu.edu

Citation:
Aquila, V., C. I. Garfinkel, P. A. Newman, L. D. Oman, and D. W. Waugh (2014), Modifications of the quasi-biennial oscillation by a geoengineering perturbation of the stratospheric aerosol layer, *Geophys. Res. Lett.*, *41*, 1738–1744, doi:10.1002/2013GL058818.

Received 22 NOV 2013
Accepted 23 JAN 2014
Accepted article online 27 JAN 2014
Published online 12 MAR 2014

Modifications of the quasi-biennial oscillation by a geoengineering perturbation of the stratospheric aerosol layer

V. Aquila[1,2], C. I. Garfinkel[3], P.A. Newman[4], L.D. Oman[4], and D.W. Waugh[2]

[1]Goddard Earth Science Technology and Research, Greenbelt, Maryland, USA, [2]Department of Earth and Planetary Sciences, Johns Hopkins University, Baltimore, Maryland, USA, [3]The Fredy and Nadine Herrmann Institute of Earth Sciences, Hebrew University, Jerusalem, Israel, [4]NASA Goddard Space Flight Center, Greenbelt, Maryland, USA

Abstract This paper examines the impact of geoengineering via stratospheric sulfate aerosol on the quasi-biennial oscillation (QBO) using the NASA Goddard Earth Observing System version 5 Chemistry Climate Model. We performed four 30 year simulations with a continuous injection of sulfur dioxide on the equator at 0° longitude. The four simulations differ by the amount of sulfur dioxide injected (5 Tg/yr and 2.5 Tg/yr) and the altitude of the injection (16 km–25 km and 22 km–25 km). We find that such an injection dramatically alters the quasi-biennial oscillation, prolonging the phase of easterly shear with respect to the control simulation. This is caused by the increased aerosol heating and associated warming in the tropical lower stratosphere and higher residual vertical velocity. In the case of maximum perturbation, i.e., highest stratospheric aerosol burden, the lower tropical stratosphere is locked into a permanent westerly QBO phase.

1. Introduction

The quasi-biennial oscillation (QBO) is an approximately 28 month period oscillation of zonally symmetric easterly and westerly winds in the tropical stratosphere. The QBO is caused by vertically propagating waves, such as equatorial Kelvin and Rossby-gravity waves, that deposit momentum in the stratosphere [e.g., *Baldwin et al*., 2001]. While the QBO is confined to the tropics, its phase affects the stratospheric transport to the extratropics and the strength of the polar vortex [*Holton and Tan*, 1980], altering transport from the tropics to middle and high latitudes of stratospheric trace gases and aerosols [*Trepte and Hitchman*, 1992]. Additionally, studies have shown that the QBO can impact the tropospheric winds [*Garfinkel and Hartmann*, 2011] and precipitation [*Jihoon et al*., 2013].

The vertical descent of the QBO wind shear is linked to the mean tropical upwelling of the Brewer-Dobson circulation (BDC) [e.g., *Watanabe and Kawatani*, 2012]. *Kawatani and Hamilton* [2013] identified in radiosonde observations for the 1953–2012 period a long-term trend of weakening QBO amplitude, which they attributed to the BDC strengthening due to increasing greenhouse gases.

Geoengineering is a deliberate modification of the Earth system in order to counteract global warming due to increasing greenhouse gases. Some proposed geoengineering methods address the causes of the warming by reducing the amount of solar radiation reaching the Earth surface (solar radiation management), for instance by continuously injecting sulfate aerosol into the stratosphere. This method aims to reproduce the global surface cooling observed after major volcanic eruptions.

In addition to its effect on tropospheric temperatures [*Kravitz et al*., 2013], precipitation [*Haywood et al*., 2013; *Tilmes et al*., 2013], and stratospheric ozone [*Pitari et al*., 2014; *Tilmes et al*., 2009], such stratospheric injection of aerosol would also lead to perturbations of stratospheric dynamics. An increase in stratospheric aerosol loading would warm the lower stratosphere, mainly via absorption of longwave radiation. Such warming would lead to a strengthening of the tropical upwelling, as showed by *Aquila et al*. [2012] in the case of a Mount Pinatubo-like eruption, which could interfere with the periodicity of the QBO. After the Mount Pinatubo eruption, observations showed a warming of the lower stratosphere of about 3 K and a delay in the downward propagation of the easterly shear [*Labitzke*, 1994].

Here we present a set of four model experiments that simulate the geoengineering stratospheric injection of sulfur dioxide, varying the burden and altitude of the SO_2 injection, in order to investigate the impact of stratospheric aerosol geoengineering on the QBO.

Table 1. Summary of the Model Experiments Performed for This Study[a]

	Injection Burden (Tg-SO_2)	Injection Altitude (km)	Aerosol Stratospheric Burden (Tg-S)	QBO Period (SD)[b] (Months)
Control	-	-	-	25.1 (4.0)
$G_{2.5}^{16-25km}$	2.5	16–25	1.5	26.8 (10.1)
$G_{2.5}^{22-25km}$	2.5	22–25	2.1	29.0 (5.4)
$G_{5}^{16-25km}$	5	16–25	3.1	50.8 (2.2)
$G_{5}^{22-25km}$	5	22–25	4.7	-

[a]The period of the QBO is calculated at 30 hPa.
[b]SD means standard deviation.

2. Model Simulations

The Goddard Earth Observing System Chemistry Climate Model (GEOSCCM) couples the GEOS-5 general circulation model [*Rienecker et al*., 2011], the Georgia Institute of Technology-Goddard Global Ozone Chemistry Aerosol Radiation and Transport (GOCART) module [*Colarco et al*., 2010], and the StratChem stratospheric chemistry module [*Pawson et al*., 2008]. GOCART is a bulk aerosol model which include a parameterization of the chemical production of SO_4 aerosol from oxidation of dimethyl sulfide (DMS) by OH during day and NO_3 during night and from oxidation of SO_2 by OH in the gas phase and by H_2O_2 in the aqueous phase. Evaluation of a similar version of GEOSCCM with respect to stratospheric aerosol by *Aquila et al*. [2012, 2013] shows good agreement with observations of aerosol distributions and ozone and NO_2 depletion after the eruption of Mount Pinatubo. Compared to *Aquila et al*. [2013], this GEOSCCM version includes both a mechanism to generate the QBO using a gravity wave drag parameterization [*Molod et al*., 2012] and a coupling between aerosol and heterogeneous chemistry via the aerosol surface area density. The aerosol surface area density is calculated from the dry sulfate mass assuming that the aerosol particles are lognormally distributed with modal radius 0.35 μm. This same size distribution, hydrated accordingly to the relative humidity, is used to calculate the optical properties of the stratospheric sulfate aerosol and its settling velocity.

The GEOSCCM resolution is 2.0° latitude by 2.5° longitude, with 72 vertical hybrid levels from surface to 0.01 hPa. The model is prescribed with sea surface temperatures and sea ice concentrations calculated with the Community Earth System Model [*Gent et al*., 2011] using emission inventories valid for the Representative Concentration Pathway (RCP) 4.5 [*Taylor et al*., 2012].

We performed four 30 year long experiments from 2020 to 2049 in which we prescribed a continuous injection of SO_2 in the stratosphere on the equator at 0° longitude. The four perturbed simulations differ from each other with regard to the burden (5 Tg/yr in two of the experiments and 2.5 Tg/yr in the other two) and altitude (16 km–25 km and 22 km–25 km) of the geoengineering injection. The four experiments ($G_5^{16-25km}$, $G_{2.5}^{16-25km}$, $G_5^{22-25km}$, and $G_{2.5}^{22-25km}$) are summarized in Table 1. $G_5^{16-25km}$ corresponds to the experiment G_4 of the Geoengineering Model Intercomparison Project [*Kravitz et al*., 2011]. Additionally, we performed a control simulation without stratospheric SO_2 injection.

We concentrate in our discussion on the last 20 years of simulations, when the sources and sinks of geoengineering aerosol are in equilibrium. During this time span, the atmospheric burden of the geoengineering sulfate aerosol is equal to 4.7 Tg-S in $G_5^{22-25km}$, 3.1 Tg-S in $G_5^{16-25km}$, 2.1 Tg-S in $G_{2.5}^{22-25km}$, and 1.5 Tg-S in $G_{2.5}^{16-25km}$ (Table 1). The mixing between the tropics and extratropics is weaker at the altitudes where the aerosol is injected in $G_5^{22-25km}$ and $G_{2.5}^{22-25km}$ than at lower altitudes (16–20 km), and this leads to longer stratospheric residence times and higher aerosol burdens in these experiments (Table 1). For comparison, *Baran and Foot* [1994] measured a maximum stratospheric aerosol burden of about 7 Tg-S after the eruption of Mount Pinatubo, which decreased to 4 Tg-S about 18 months after the eruption. The vertical distribution of the geoengineering aerosol in the four simulations is shown in Figure S1 in the supporting information. The total burden in our simulations is similar to that in the geoengineering experiments of *Heckendorn et al*. [2009], but the aerosols are more confined to the tropics in our simulations. This is likely due to differences in the transport (*Heckendorn et al*. [2009] use a two-dimensional model) but could also be due to differences in the injection height and microphysical processes.

The stratospheric aerosol optical thickness (AOT) can be roughly converted to radiative forcing by multiplying by 25 W/m^2 [*Hansen et al*., 2005]. Using this conversion factor, the aerosol radiative forcing in our simulations

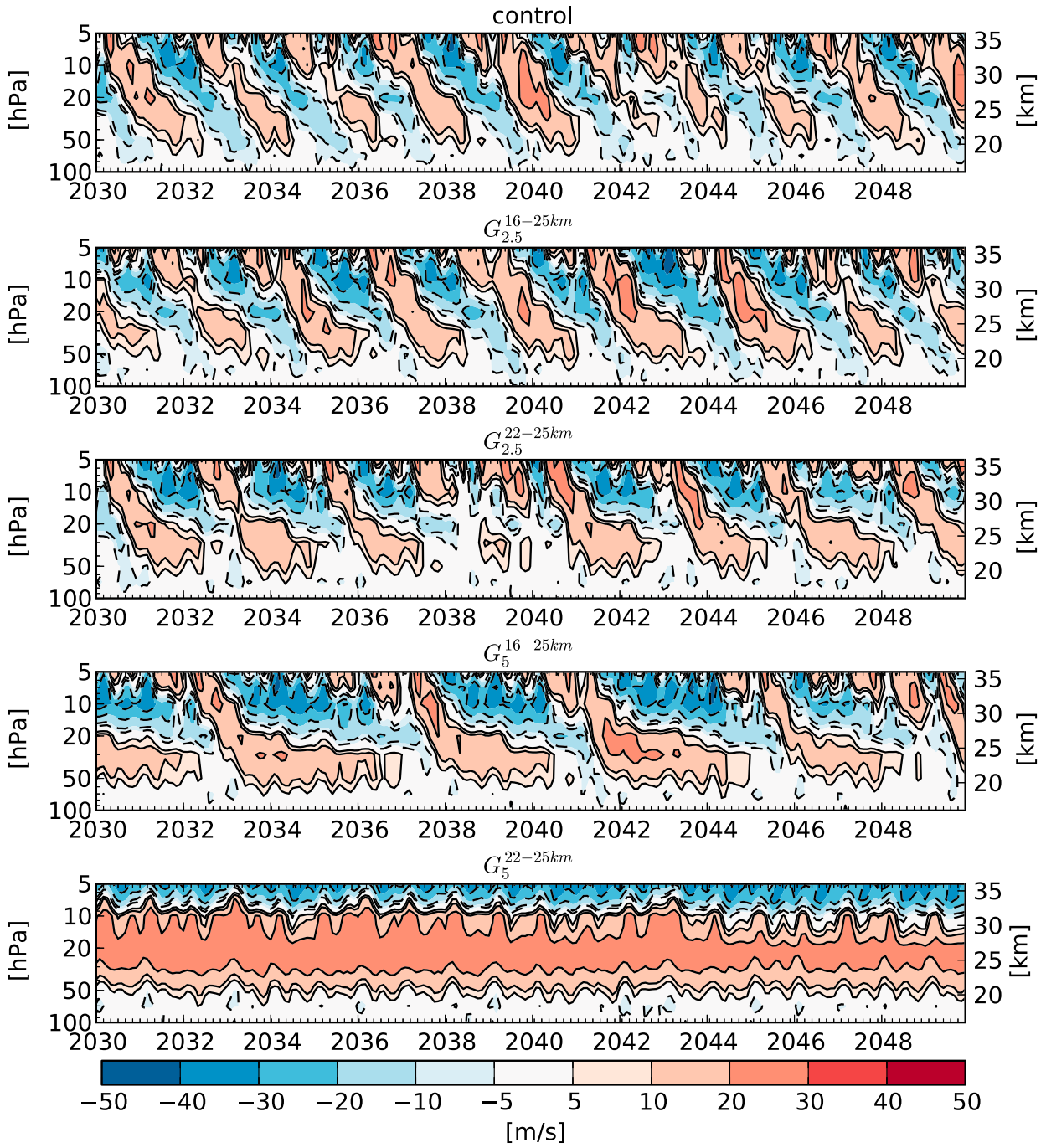

Figure 1. Vertical profiles of the zonal wind, zonally averaged between 2°S and 2°N in (from top to bottom) control run, $G_{2.5}^{16-25km}$, $G_{2.5}^{22-25km}$, $G_{5}^{16-25km}$, and $G_{5}^{22-25km}$.

ranges from $-1 Wm^{-2}$ in $G_{2.5}^{16-25km}$ to $-3\ Wm^{-2}$ in $G_{5}^{22-25km}$ (see Figure S2 supporting information for the simulated AOT). Even in a fairly optimistic scenario such as the Representative Concentration Pathways (RCP) 4.5 [*Clarke et al.*, 2007; *Smith and Wigley*, 2006; *Wise et al.*, 2009], the radiative forcing by increasing greenhouse gases reaches $3 Wm^{-2}$ around 2030. Hence, the aerosol perturbations introduced in our experiments are within the possible range that might be needed to offset warming from increasing greenhouse gases.

Note that in these experiments, the source function for gravity waves is held fixed and is not coupled to convection, and the sea surface temperatures (SSTs) do not vary among the experiments. It is likely that the

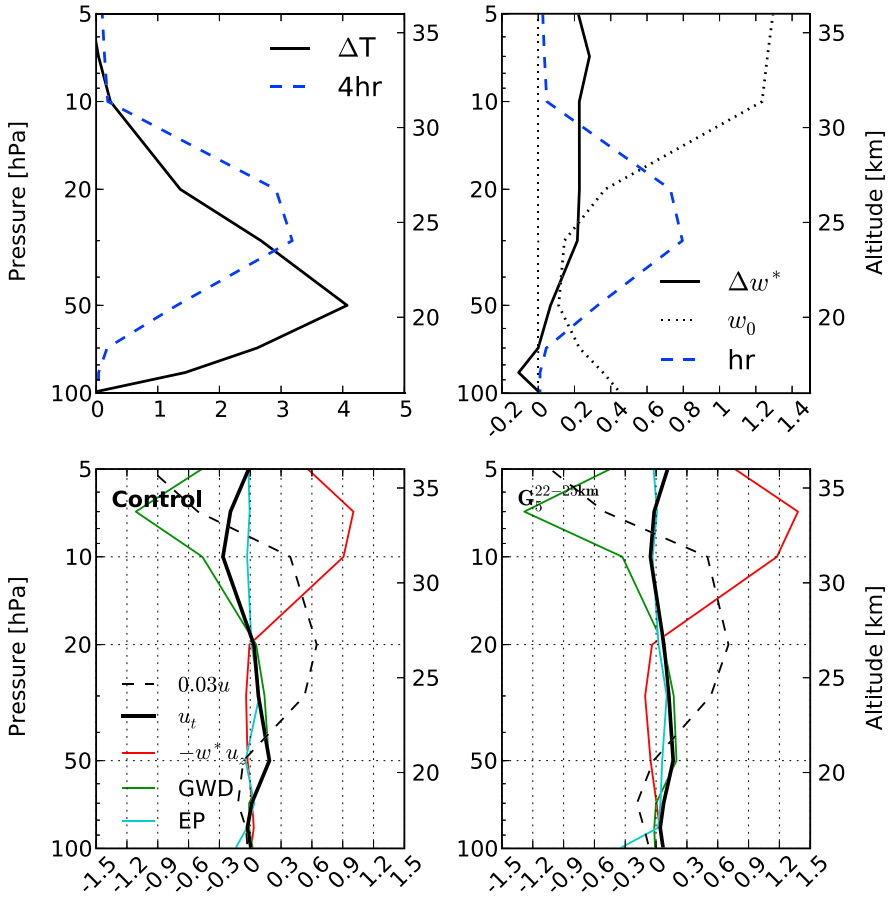

Figure 2. (top row) Vertical profiles of the zonal mean (2°S–2°N) anomaly of the temperature (K (left)) and residual vertical velocity (mm/s (right)). The anomalies are calculated between the 2 months of the control and $G_5^{22-25km}$ when the *u* wind profiles are the most similar. The dashed blue line shows the aerosol heating rates in K/d in $G_5^{22-25km}$ (note the scaling factor in the top left figure). The dotted black line in the top right figure shows $\overline{w}^*$ in the control simulation. (bottom row) Vertical profiles of the forcing terms (in m s^{-1} d^{-1}) that drive the QBO in the (left) control and (right) $G_5^{22-25km}$ simulations during the months considered in Figure 2 (top row). Shown are the 2°S–2°N zonal means of *u* wind in m/s multiplied by a factor 0.03 (dashed black), the time derivative of *u* (solid black), the advection of the mean flow (red), the parameterized gravity wave drag (green), and the divergence of the Eliassen-Palm flux (blue).

SSTs and the convection will change were geoengineering implemented. Hence, the source of wave driving for the QBO in these experiments does not vary realistically in response to geoengineering, and future work is necessary to explore whether these limitations affect the model results presented below.

3. Results

Our results show that the stratospheric aerosol injection dramatically perturbs the QBO periodicity, prolonging the phase of easterly shear with respect to the control case. Figure 1 shows the vertical profiles of the tropical zonal wind, averaged between 2°S and 2°N, in the control simulation (top) and in the four geoengineering experiments. The phase of easterly shear persists for longer and longer with increasing stratospheric burden of aerosol. Table 1 reports the mean value and standard deviation of the simulated QBO period: the period of the QBO increases with the burden of geoengineering aerosol, from about 25 months in the control simulation to about 50 months in $G_5^{16-25km}$. The QBO completely disappears in $G_5^{22-25km}$ (bottom), where the stratosphere is in a perpetual easterly shear or westerly phase. In the following discussion we will focus on $G_5^{22-25km}$. The response of the QBO to the increase of aerosol is fast, within one QBO period in the G_5 experiments, and within two QBO periods in $G_{2.5}$. Additionally, between 17 km and 30 km altitude the amplitude of the QBO decreases with increasing stratospheric aerosol burden (Figure S3 in the supporting information).

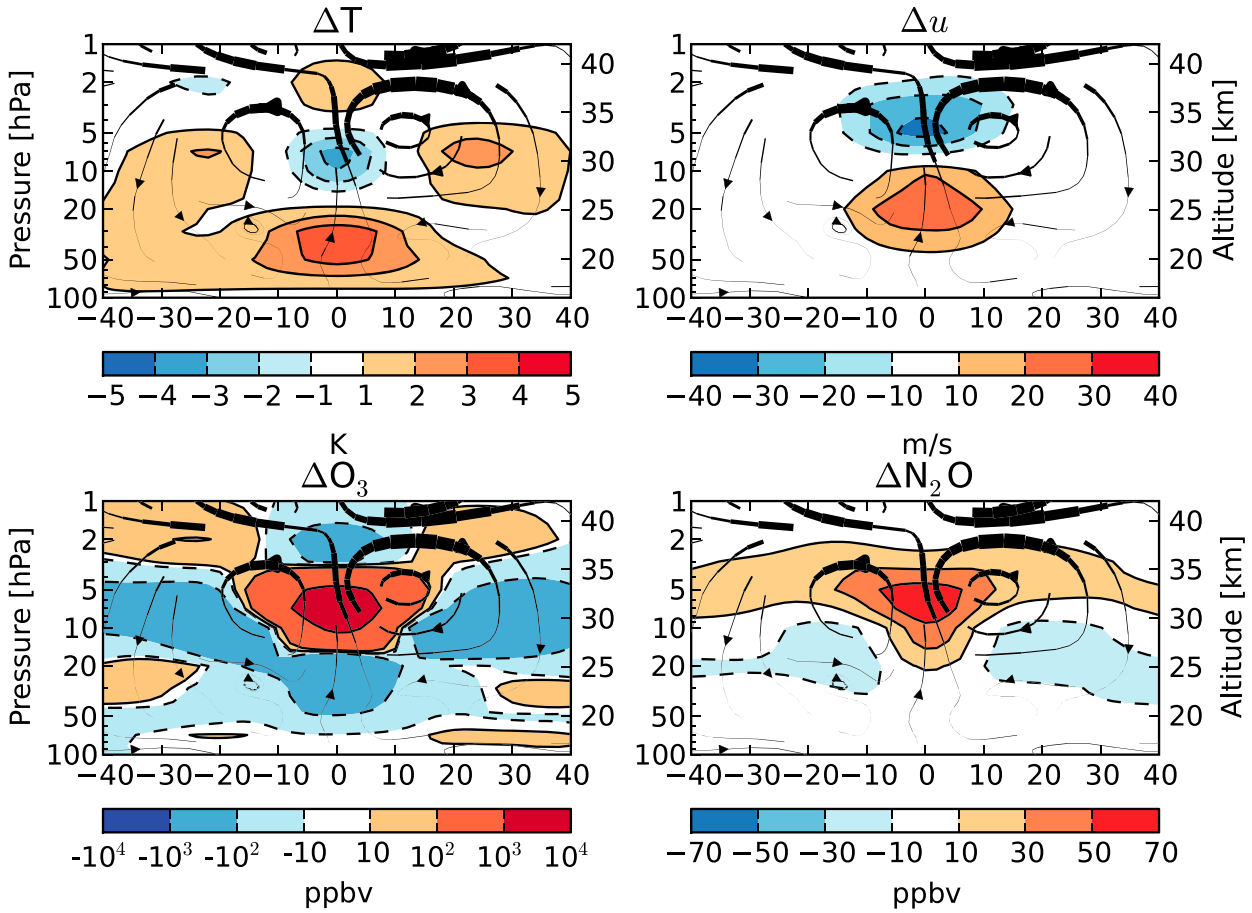

Figure 3. Vertical profiles of the zonal mean anomalies of temperature, zonal wind *u*, ozone, and N_2O concentrations in $G_5^{22-25km}$ with respect to the control simulation. The streamlines show the anomaly of the residual circulation. The anomalies are calculated over the whole 2030–2050 period. The thickness of the streamlines is proportional to the change of speed.

Figure 2 shows the mechanism that leads to the interruption of the QBO in $G_5^{22-25km}$. The heating from the geoengineering aerosol induces a warming of the lower stratosphere up to about 27 km altitude (Figure 2, top left). Because the radiative damping timescales are longer in the lower stratosphere than in the upper stratosphere, the aerosols affect lower stratospheric temperature more strongly [*Newman and Rosenfield*, 1997]. The warmer temperature centered on the equator induces an equatorial positive wind shear $\left(\beta\overline{u}_z = -R\overline{T}_{yy}/H\right)$, which results in persistent westerly winds between 20 and 30 km. The heating anomaly due to the aerosol also causes an increase of the residual vertical velocity $\overline{w}^*$ (Figure 2, top right), which advects the aerosol upward from the initial injection altitude. The increase in $\overline{w}^*$ extends well above the level at which the diabatic heating ends, consistent with *Holloway and Neelin* [2007] and *Garfinkel et al*. [2013].

The typical processes that lead to the QBO's downward propagation weaken in the presence of the increase to $\overline{w}^*$ due to the geoengineering aerosols. This effect is demonstrated in Figure 2 (bottom row), which show the budget of the terms that force the QBO in the control and $G_5^{22-25km}$ experiments, averaged between 2°S and 2°N. When the QBO propagates downward, momentum deposition from the parameterized gravity waves (GWD) drives the downward propagation, but it is opposed (but not fully) by westerly momentum from the vertical advection of the mean flow $\left(-\overline{w}^*\overline{u}_z\right)$ which advects the wind anomalies upward. In the presence of aerosols and enhanced $\overline{w}^*$, the easterly momentum from the parameterized gravity waves (GWD) and the westerly momentum from the vertical advection of the mean flow $\left(-\overline{w}^*\overline{u}_z\right)$ balance each other leading to a smaller time derivative of the zonal wind.

Figure 3 shows the anomalies of temperature, zonal winds, and ozone and N_2O concentrations in $G_5^{22-25km}$ with respect to the control simulation. The circulation anomaly is also superimposed in Figure 3. The temperature anomalies (Figure 3, top left) show the largest warming centered at about 20 km and related to the

absorption of longwave radiation by the aerosol. The cold anomaly above this region near 30 km is related to the circulation anomaly caused by the aerosol. This induced circulation is also clearly reflected in the N_2O concentrations (Figure 3, bottom right). N_2O is a well-suited tracer to study stratospheric transport, due to its long stratospheric lifetime and its distribution with higher concentrations at the surface in the tropics. The circulation changes induced by the aerosol increase the N_2O concentrations in the middle stratosphere and enhance its transport to the extratropics. The ozone anomalies (Figure 3, bottom left) are due to a combination of heterogeneous chemistry on the aerosol particles and to the induced change in tropical dynamics [*Aquila et al*., 2013; *Pitari et al*., 2014], which advects air with different ozone concentrations. Similar changes are also found in the other simulations (see supporting information); there are some differences in the spatial structure of the anomalies among the experiments, and future work is needed to examine these differences

4. Conclusions

Our simulations show that geoengineering injection of stratospheric aerosol can lead to dramatic changes in the QBO, prolonging the phase of easterly shear with respect to the control simulation. For very large increases in stratospheric aerosol burden (4.7 Tg-S), the lower tropical stratosphere is locked into a permanent westerly QBO phase. Figure S7 in the supporting information suggests that there is roughly a quadratic relationship between the aerosol burden and the QBO period, calculated at 30 hPa. This modification of the QBO occurs because the increase in aerosol burden leads to a warming of the tropical lower middle stratosphere mainly via absorption of longwave radiation, and hence to stronger westerly winds resulting from the thermal wind relation. This warming also induces an increase in the residual vertical velocity $\overline{w}^*$, which broadens the band of westerly winds and lofts the aerosol higher in the stratosphere. Because the QBO can impact stratospheric and tropospheric ozone [*Randel and Wu*, 1996; *Ziemke and Chandra*, 1999; *Oman et al*., 2013], tropospheric winds [*Garfinkel and Hartmann*, 2011], and precipitation [*Jihoon et al*., 2013], this geoengineering-forced permanent lower stratospheric QBO westerly phase could substantially alter surface climate.

Acknowledgments
Simulations performed by V. Aquila were supported by the NASA High-End Computing (HEC) Program through the NASA Center for Climate Simulations (NCCS) at Goddard Space Flight Center.

The Editor thanks Scott Osprey and an anonymous reviewer for their assistance in evaluating this paper.

References

Aquila, V., L. D. Oman, R. S. Stolarski, P. R. Colarco, and P. A. Newman (2012), Dispersion of the volcanic sulfate cloud from a Mount Pinatubo-like eruption, *J. Geophys. Res.*, *117*, D06216, doi:10.1029/2011JD016968.

Aquila, V., L. D. Oman, R. Stolarski, A. R. Douglass, and P. A. Newman (2013), The response of ozone and nitrogen dioxide to the eruption of Mt. Pinatubo at southern and northern midlatitudes, *J. Atmos. Sci.*, *70*(3), 894–900, doi:10.1175/JAS-D-12-0143.1.

Baldwin, M. P., et al. (2001), The quasi-biennial oscillation, *Rev. Geophys.*, *39*(2), 179–229, doi:10.1029/1999RG000073.

Baran, A. J., and J. S. Foot (1994), New application of the operational sounder HIRS in determining climatology of sulphuric acid aerosol from the Pinatubo eruption, *J. Geophys. Res.*, *99*(D12), 25,673–25,679, doi:10.1029/94JD02044.

Clarke, L., J. Edmonds, H. Jacoby, H. Pitcher, J. Reilly, and R. Richels (2007), Scenarios of greenhouse gas emissions and atmospheric concentrations, 154 pp., Sub-report 2.1A of Synthesis and Assessment Product 2.1 by the U.S. Climate Change Science Program and the Subcommittee on Global Change Research, Department of Energy, Office of Biological & Environmental Research, Washington, D.C.

Colarco, P., A. Da Silva, M. Chin, and T. Diehl (2010), Online simulations of global aerosol distributions in the NASA GEOS-4 model and comparisons to satellite and ground-based aerosol optical depth, *J. Geophys. Res.*, *115*, D14207, doi:10.1029/2009JD012820.

Garfinkel, C. I., and D. L. Hartmann (2011), The influence of the quasi-biennial oscillation on the troposphere in winter in a hierarchy of models, Part I: Simplified dry GCM runs, *J. Atmos. Sci.*, *68*(6), 1273–1289, doi:10.1175/2011JAS3665.1.

Garfinkel, C. I., D. W. Waugh, L. D. Oman, L. Wang, and M. M. Hurwitz (2013), Temperature trends in the tropical upper troposphere and lower stratosphere: Connections with sea surface temperatures and implications for water vapor and ozone, *J. Geophys. Res. Atmos.*, *118*, 9658–9672, doi:10.1002/jgrd.50772.

Gent, P. R., et al. (2011), The Community Climate System Model Version 4, *J. Clim.*, *24*(19), 4973–4991, doi:10.1175/2011JCLI4083.

Hansen, J., et al. (2005), Efficacy of climate forcings, *J. Geophys. Res.*, *110*, D18104, doi:10.1029/2005JD005776.

Haywood, J. M., A. Jones, N. Bellouin, and D. Stephenson (2013), Asymmetric forcing from stratospheric aerosols impacts Sahelian rainfall, *Nat. Clim. Change*, *3*, 660–665, doi:10.1038/nclimate1857.

Heckendorn, P., D. Weisenstein, S. Fueglistaler, B. P. Luo, E. Rozanov, M. Schraner, L. W. Thomason, and T. Peter (2009), The impact of geoengineering aerosols on stratospheric temperature and ozone, *Environ. Res. Lett.*, *4*, 045,108, doi:10.1088/1748-9326/4/4/045108.

Holloway, C. E., and J. D. Neelin (2007), The convective cold top and quasi equilibrium, *J. Atmos. Sci.*, *64*(5), 1467–1487, doi:10.1175/JAS3907.1.

Holton, J. R., and H. C. Tan (1980), The influence of the equatorial quasi-biennial oscillation on the global circulation at 50 mb, *J. Atmos. Sci.*, *37*, 2200–2208, doi:10.1175/1520-0469(1980)037<2200:TIOTEQ>2.0.CO;2.

Jihoon, S., W. Choi, D. Youn, D.-S. R. Park, and J. Y. Kim (2013), Relationship between the stratospheric quasi-biennial oscillation and spring rainfall in the western North Pacific, *Geophys. Res. Lett.*, *40*, 5949–5953, doi:10.1002/2013GL058266.

Kawatani, Y., and K. Hamilton (2013), Weakened stratospheric quasibiennial oscillation driven by increased tropical mean upwelling, *Nature*, *497*(7450), 478–481, doi:10.1038/nature12140.

Kravitz, B., A. Robock, O. Boucher, H. Schmidt, K. E. Taylor, G. Stenchikov, and M. Schulz (2011), The Geoengineering Model Intercomparison Project (GeoMIP), *Atmos. Sci. Let.*, *12*(2), 162–167, doi:10.1002/asl.316.

Kravitz, B., et al. (2013), Climate model response from the Geoengineering Model Intercomparison Project (GeoMIP), *J. Geophys. Res. Atmos.*, *118*, 1–13, doi:10.1002/jgrd.50646.

Labitzke, K. (1994), Stratospheric temperature changes after the Pinatubo eruption, *J. Atmos. Terr. Phys.*, *56*(9), 1027–1034, doi:10.1016/0021-9169(94)90039-6.

Molod, A., L. Takacs, M. Suarez, J. Bacmeister, I.-S. Song, and A. Eichmann (2012), The GEOS-5 Atmospheric General Circulation Model: Mean climate and development from MERRA to Fortuna, Technical Report Series on Global Modeling and Data Assimilation, 28, NASA, Greenbelt, Md.

Newman, P. A., and J. E. Rosenfield (1997), Stratospheric thermal damping times, *Geophys. Res. Lett.*, *24*(4), 433–436, doi:10.1029/96GL03720.

Oman, L. D., A. R. Douglass, J. R. Ziemke, J. M. Rodriguez, D. W. Waugh, and J. E. Nielsen (2013), The ozone response to ENSO in Aura satellite measurements and a chemistry-climate simulation, *J. Geophys. Res. Atmos.*, *118*, 965–976, doi:10.1029/2012JD018546.

Pawson, S., R. S. Stolarski, A. R. Douglass, P. A. Newman, J. E. Nielsen, S. M. Frith, and M. L. Gupta (2008), Goddard Earth Observing System chemistry-climate model simulations of stratospheric ozone-temperature coupling between 1950 and 2005, *J. Geophys. Res.*, *113*, D12103, doi:10.1029/2007JD009511.

Pitari, G., V. Aquila, B. Kravitz, A. Robock, S. Watanabe, I. Cionni, N. De Luca, G. Di Genova, E. Mancini, and S. Tilmes (2014), Stratospheric ozone response to sulfate geoengineering: Results from the Geoengineering Model Intercomparison Project (GeoMIP), *J. Geophys. Res. Atmos.*, doi:10.1002/2013JD020566.

Randel, W. J., and F. Wu (1996), Isolation of the ozone QBO in SAGE II data by singular-value decomposition, *J. Atmos. Sci.*, *53*(17), 2546–2559, doi:10.1175/1520-0469(1996)053%3C2546:IOTOQI%3E2.0.CO;2.

Rienecker, M. M., M. J. Suarez, R. Gelaro, R. Todling, J. Bacmeister, E. Liu, et al. (2011), MERRA: NASA's Modern-Era Retrospective Analysis for Research and Applications, *J. Clim.*, *24*(14), 3624–3648, doi:10.1175/JCLI-D-11-00015.1.

Smith, S. J., and T. M. L. Wigley, (2006), Multi-gas forcing stabilization with the MiniCAM, *Energy J.*, (Special Issue #3), 373–391, doi:10.5547/ISSN0195-6574-EJ-VolSI2006-NoSI3-19.

Taylor, K. E., R. J. Stouffer, and G. A. Meehl (2012), An overview of CMIP5 and the experiment design, *Bull. Am. Meteorol. Soc.*, *93*, 485–498, doi:10.1175/BAMS-D-11-00094.1.

Tilmes, S., R. R. Garcia, D. E. Kinnison, A. Gettelman, and P. J. Rasch (2009), Impact of geoengineered aerosols on the troposphere and stratosphere, *J. Geophys. Res.*, *114*, D12305, doi:10.1029/2008JD011420.

Tilmes, S., et al. (2013), The hydrological impact of geoengineering in the Geoengineering Model Intercomparison Project (GeoMIP), *J. Geophys. Res. Atmos.*, *118*, 11,036–11,058, doi:10.1002/jgra.50868.

Trepte, C. R., and M. H. Hitchman (1992), Tropical stratospheric circulation deduced from satellite aerosol data, *Nature*, *335*, 626–628, doi:10.1038/355626a0.

Watanabe, S., and Y. Kawatani (2012), Sensitivity of the QBO to mean tropical upwelling under a changing climate simulated with an Earth system model, *J. Meteorol. Soc. Jpn.*, *90A*(0), 351–360, doi:10.2151/jmsj.2012-A20.

Wise, M. A., K. V. Calvin, A. M. Thomson, L. E. Clarke, B. Bond-Lamberty, R. D. Sands, S. J. Smith, A. C. Janetos, and J. A. Edmonds (2009), Implications of limiting CO_2 concentrations for land use and energy, *Science*, *324*, 1183–1186, doi:10.1126/science.1168475.

Ziemke, J. R., and S. Chandra (1999), Seasonal and interannual variabilities in tropical tropospheric ozone, *J. Geophys. Res.*, *104*(D17), 21,425–21,442, doi:10.1029/1999JD900277.